# Ag+ Ion Binding to Human Metallothionein-2A Is Cooperative and Domain Specific

**Shiyu Dong**,
Department of Chemistry, Texas A&M University, College Station, Texas 77843, United States

**Mehdi Shirzadeh**,
Department of Chemistry, Texas A&M University, College Station, Texas 77843, United States

**Liqi Fan**,
Department of Chemistry, Texas A&M University, College Station, Texas 77843, United States

**Arthur Laganowsky**,
Department of Chemistry, Texas A&M University, College Station, Texas 77843, United States

**David H. Russell**
Department of Chemistry, Texas A&M University, College Station, Texas 77843, United States

## Abstract

Metallothioneins (MTs) constitute a family of cysteine-rich proteins that play key biological roles for a wide range of metal ions, but unlike many other metalloproteins, the structures of apo- and partially metalated MTs are not well understood. Here, we combine nano-electrospray ionization-mass spectrometry (ESI-MS) and nano-ESI-ion mobility (IM)-MS with collision-induced unfolding (CIU), chemical labeling using $N$-ethylmaleimide (NEM), and both bottom-up and top-down proteomics in an effort to better understand the metal binding sites of the partially metalated forms of human MT-2A, viz., $Ag_4$-MT. The results for $Ag_4$-MT are then compared to similar results obtained for $Cd_4$-MT. The results show that $Ag_4$-MT is a cooperative product, and data from top-down and bottom-up proteomics mass spectrometry analysis combined with NEM labeling revealed that all four $Ag^+$ ions of $Ag_4$-MT are bound to the $\beta$-domain. The binding sites are identified as Cys13, Cys15, Cys19, Cys21, Cys24, and Cys26. While both $Ag^+$ and $Cd^{2+}$ react with MT to yield cooperative products, i.e., $Ag_4$-MT and $Cd_4$-MT, these products are very different; $Ag^+$ ions of $Ag_4$-MT are located in the $\beta$-domain, whereas $Cd^{2+}$ ions of $Cd_4$-MT are located in the $\alpha$-domain. $Ag_6$-MT has been reported to be fully metalated in the β-domain, but our data suggest the two additional Ag+ ions are more weakly bound than are the other four. Higher

**Corresponding Author** David H. Russell – Department of Chemistry, Texas A&M University, College Station, Texas 77843, United States; russell@chem.tamu.edu.

order $Ag_i$-MT complexes ($i = 7–17$) are formed in solutions that contain excess $Ag^+$ ions, and these are assumed to be bound to the $\alpha$-domain or shared between the two domains. Interestingly, the excess $Ag^+$ ions are displaced upon addition of NEM to this solution to yield predominantly $Ag_4NEM_{14}$-MT. Results from CIU suggest that $Ag_i$-MT complexes are structurally more ordered and that the energy required to unfold these complexes increases as the number of coordinated $Ag^+$ increases.

## Graphical Abstract
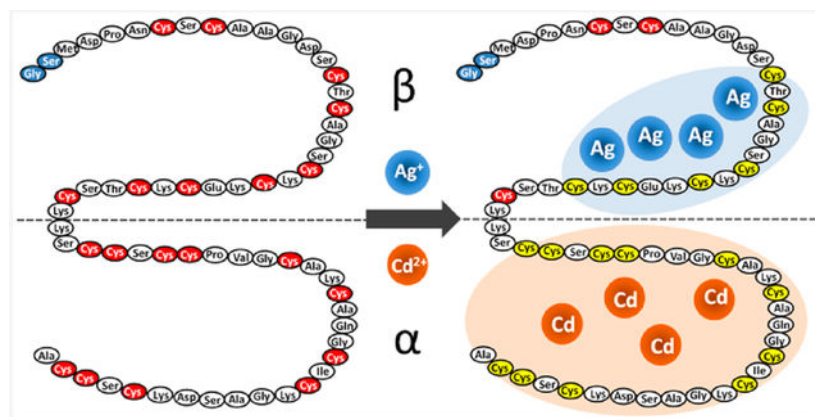


Metallothioneins (MTs) constitute a family of cysteine-rich small proteins that bind a wide range of metal ions.[1-3] While the exact biological function(s) of MTs are not fully understood, they have been implicated in diseases such as Alzheimer's, Parkinson's, and cancer, which suggests that MTs have functions other than being "sponges" for metal homeo-stasis, heavy metal detoxification, and antioxidation.[1,4-8] Studies of structure/function relationships of MTs are complicated by the fact that the physiologically dominant forms of MTs are the apo and partially metalated forms,[9-12] but their low abundances and conformational heterogeneity have limited the in vitro studies of partially metalated MTs using traditional structural approaches, viz., X-ray cryptography or NMR spectroscopy.[1] Apo-MTs lack well-defined tertiary structure, and structure(s) and folding stabilities of metalated species are largely determined by metal–thiolate bonds.[1,13] Structural characterization of metalated MTs has proved challenging, owing to difficulties associated with growing high-quality crystals required for X-ray crystallography. It has been equally difficult to locate metal bound cysteine residues using conventional protein NMR spectroscopy.[1,2] While it is possible to substitute NMR silent metal ions with NMR active nuclei, i.e., $Zn^{2+}$ by $^{111}Cd^{2+}$ or $^{113}Cd^{2+}$[13] and $Cu^+$ by $^{109}Ag^+$,[14] it is unclear that such replacements are isostructural.[1] There is strong evidence that binding of MTs involves two domains and that $Cd^{2+}$ and $Zn^{2+}$ form $M_4Cys_{11}$ clusters in the $\alpha$-domain and $M_3Cys_9$ clusters in the $\beta$-domain.[1,13,15,16] Both $Cd^{2+}$ and $Zn^{2+}$ adopt tetrahedral coordination spheres with each metal ion coordinated to four thiolates; however, the coordination of monovalent metal ions, i.e., $Ag^+$ and $Cu^+$, is more likely to involve digonal and/or trigonal geometries.[17,18] The redox-stable monovalent $Ag^+$ was previously used to model redox-active $Cu^+$–MT complexes;[14,17,19] however, Ag-MT and Cu-MT differ significantly in terms of metalation and binding geometries.[19] For example, Scheller et al.[20] reported that up to 20

$Cu^+$ ions bind to MT, whereas Zelazowski[21] and Scheuhammer and Cherian[22] reported that 17–18 $Ag^+$ ions bind to MT. The structures for Cu-MT and Ag-MT complexes from *Saccharomyces cerevisiae* have been reported by Bertini et al.[23] and Narula et al.[14] Both $Cu^+$ and $Ag^+$ adopt mixed trigonal planar and linear/digonal coordination; however, the reported structures are not identical.[23] X-ray absorption spectroscopy has been used to study the binding geometries of $Cu^+$ and $Ag^+$ for mammalian MT; $Cu^+$ is more likely to adopt trigonal geometry, while $Ag^+$ is reported to occupy trigonal and digonal coordination.[24,25]

In recent years, there has been growing interest in using mass spectrometry for studies of metalloproteins. Fenselau and co-workers were one of the first to employ electrospray ionization-mass spectrometry (ESI-MS) for studies of MTs.[26,27] Increasing numbers of investigators have incorporated ESI-MS in their studies. Kagi and Vallee reported one of the earliest attempts to isolate MT from equine renal cortex,[28] and Kagi and co-workers have reported important applications of both NMR[13,29,30] and MS[31] for studies of structure of $Cd_7$-MT and cooperativity of metalation. Lobinski and co-workers used both microscale purification techniques (HPLC, capillary electrochromatography) and trace analysis techniques, including ESI-MS, to successfully detect MT isoforms from different systems.[32-34] Atrian, Capdevila, and co-workers used ESI-MS to investigate metal binding of MT from different species and to bridge the gap between phytochelatins and metal-lothions.[35-38] Stillman and co-workers have made extensive use of ESI-MS for studies of ion reactivity and kinetics in metalation reactions of MT employing a broad range of metal ions.[39-41] Blindauer and co-workers have reported MT expression in different species and dynamics of metal binding and release employing multiple analytical methods including MS.[42-44]

While ESI-MS is able to distinguish different metalated species on the basis of mass-to-charge ratios, the mass spectra do not provide information related to metal ion binding sites, structural changes that accompany metal ion binding, or stabilities of the metal–MT complexes. Here, a comprehensive strategy employing both ESI mass spectrometry and ESI ion mobility-mass spectrometry (IM-MS) is used to investigate $Ag^+$ binding to human MT-2A (denoted as MT). The major products formed upon addition of $Ag^+$ to MT are $Ag_i$-MT ($i = 4$–17). The results presented provide clear evidence that the cooperative binding product, viz., $Ag_4$-MT, is formed by domain-specific metal ion binding to the $\beta$-domain, unlike the similar cooperative binding product, $Cd_4$-MT, which is formed by the addition of $Cd^{2+}$ to the $\alpha$-domain.[45] Additional evidence for domain specific binding for $Ag^+$ and $Cd^{2+}$ to MT is obtained by mixed metalation reactions.[46] The combination of nano-ESI and IM-MS affords direct measurements of the ion shape/size as well as conformational diversity of the ion population,[47-50] which can be compared to conformational preferences of apo- and partially metalated MT.[45,46,51-53] Prior studies have shown that, under suitable instrumental conditions, it is possible to maintain noncovalent interactions as well as metal–ligand interactions formed in MTs.[46, 51,54] Proteomics strategies, including "bottom-up" and "top-down", are used in concert with *N*-ethylmaleimide (NEM) labeling to ascertain the domain specific metalation that yields $Ag_4$-MT. [1,19,55,56] IM-MS is also used to perform collision-induced unfolding (CIU) experiments on $Ag_4$-MT as well as the higher metalated species $Ag_i$-MT ($i = 5$–17), which provide information for the relative stabilities of the gas-phase ions.[48,49,57-62]

## EXPERIMENTAL SECTION

Silver acetate, cadmium acetate, ammonium acetate, zinc acetate, diethylenetriaminepentaacetic acid (DTPA), dithio-threitol (DTT), tris (2-carboxyethyl) phosphine hydrochloride (TCEP), and *N*-ethylmaleimide (NEM) were purchased from Sigma-Aldrich (St. Louis, MO). Sequencing grade modified trypsin was purchased from Thermo Fisher Scientific (Waltham, MA). Deionized water (18.2 MΩ) was obtained from a Milli-Q water apparatus (Millipore, Billerica, MA). Micro Bio-Spin 6 columns were purchased from Bio-Rad Laboratories, Inc. (Hercules, CA). Details for MT expression and purification, $Zn_7$-MT demetalation, and in solution digestion for bottom-up proteomics are included in the Supporting Information.

The $Ag^+$ metalation experiment was performed by sequential addition of 1.75 $\mu$L of 1 mM (1:1 molar ratio of $Ag^+$/apo-MT, denoted as one equivalent) silver acetate to 100 $\mu$L of MT solution until the metalation degree of products showed saturation.[45] After each $Ag^+$ addition, the solution was incubated at room temperature for 1 h and then analyzed by nESI-MS. All experiments were performed on a Waters Synapt-G2 HDMS instrument (Manchester, UK). Instrumental conditions were tuned to minimize collisional heating as previously described.[52] All ESI-MS experiments were carried out using nano-ESI capillaries (pulled borosilicate emitter tips ranging in size (IDs ~ 5–10 $\mu$m), which provide more reproducible mass spectra containing much less background noise.

A Ag/Cd mixture solution was prepared by mixing 1 mM silver acetate and 1 mM cadmium acetate solution in 1:1 ratio. Apo-MT was mixed with 7 equiv of the Ag/Cd mixture and incubated at room temperature for 1 h before analysis. The Ag/Cd mixed metal synthesis experiment was performed by adding ~3.5 equiv of 1 mM $Ag^+$ to apo-MT and incubating for 1 h at room temperature. Afterward, 3.5 equiv of 1 mM $Cd^{2+}$ was added, and the sample was incubated for 1 h at room temperature. Mass spectra and CIU heat maps of the product ions were obtained. A similar set of experiments, which involved switching the order of the addition of $Ag^+$ and $Cd^{2+}$, was performed.

$Ag_4$-MT was obtained by metalation of apo-MT (adding 7 $\mu$L of 1 mM $Ag^+$ to a 17.5 $\mu$M apo-MT solution). Four $\mu$L of 10 mM NEM was added to $Ag_4$-MT and incubated for 1 h at room temperature to completely react with metal-free cysteinyl groups. The alkylated metalated products ($Ag_4NEM_{14}$-MT) were mass-selected for direct sequencing by tandem mass spectrometry (top-down approach). The approach used to characterize metal binding sites is a combination of MS, CID, IM, and MS, denoted as MS-CID-IM-MS.[45,63-65] In this approach, CID fragment ions are dispersed in two dimensions, size-to-charge (IM) and mass-to-charge (MS). Fragment ions of different charge states fall along different trend lines in the resulting 2D spectra, which reduces spectra congestion and simplifies identification of the fragment ions.

nESI-CIU-MS experiments were carried out as described previously.[46,50] Different collision voltages were applied by changing the voltage drop (increments of 5 V) between the exit of the quadrupole and the entrance to the TWIG-trap; thus, collision energy is reported as lab-frame collision energy ($E_{lab}$).[46,54] Ion mobility profiles under different activation energy

were compiled into CIU heat maps using CIUSuite as described by Ruotolo and co-workers. [66] CIU50 data were extracted with CIUSuite2 to compare the unfolding energy. [67] Averages and standard deviations were calculated using three acquisitions. The standard deviations are within 3%.

## RESULTS AND DISCUSSION

Previous studies have illustrated the utility of nESI-MS and IMS for studies of MT. [1,45,51-53] nESI-MS allows detection and separation of each partially metalated MT species, while IMS provides information on the shape and size of each of partially and higher order metalated MT. [46] The integrated IM-MS experiments combined with covalent chemical labeling with NEM, top-down and bottom-up proteomics with MS-CID-IM-MS, and collision-induced unfolding (CIU) are designed to better assign metal ion binding site, structure, and stabilities of products formed by reactions of $Ag^+$ with MT. Rotationally averaged collision cross section (CCS) profiles obtained by ion mobility for the $5^+$ apo-MT ions are multicomponent, a signature for a conformational heterogeneity, whereas those for $4^+$ apo-MT ions are narrow, indicative of an ion population that contains less conformational diversity. [68,69] Owing to differences in the conformational diversities of the ion population, the following sections are focused exclusively on the metalation reactions of the $MT^{5+}$ ions. It should be noted however that the rates of reactions and the number of metal ions added to MT are similar for both charge states.

### Synthesis of Human $Ag_i$-MT Complexes.

Titration can be used to measure the kinetics of the metalation reactions, thereby identifying cooperative binding behavior. [3] Figure 1 contains mass spectra acquired from $Ag^+$ ion titration of human MT. Although the spectral congestion that arises from the formation of adduct ions (e.g., $Na^+$, acetate ions, and oxidized MT) and the metalated ($Ag_iMT^{5+}$) product ions complicate accurate kinetic measurements, the combined use of IMS and high mass resolution is sufficient to allow for high confidence level assignment of the product ions. [63,64,70] With increasing concentration of $Ag^+$ in MT solution, the abundances and numbers of metalated product ions increased. Upon addition of solutions containing $Ag^+$ ions, low abundance signals corresponding to $Ag_iMT$ ($i = 1-3$) and much higher abundance ions corresponding to $Ag_4$-MT are detected. The low abundance of $Ag_i$-MT ($i = 1-3$) is not surprising owing to the high concentrations of thiol ligands (20 SH group per MT molecule) as well as a high degree of cooperativity for the formation of the $Ag_4$-MT product ion. Similarly, the abundance of the $i = 5$ complex is low while that for $i = 6$ is relatively high. A progression of larger complexes is formed up to $i = 17$. It appears that the maximum number of $Ag^+$ ions that can bind to MT is different when using different experimental approaches. [19,21,22,71] Zelazowski et al. [21] used circular dichroism and luminescence spectra while Scheuhammer and Cherian [22] developed a Ag saturation assay to study Ag binding, and they all reported values similar to those reported here.

### $Ag^+$ Displacement by a Reaction with *N*-Ethyl-maleimide (NEM).

NEM displacement studies were performed on the $Ag_i$-MT ($i = 9-14$) (see Figure S1). The addition of ~20 equiv of NEM to a solution containing $Ag_i$-MT ($i = 9-14$) yielded high

abundances of $Ag_4NEM_{14}$-MT. The results for the displacement of $Ag^+$ by NEM provide additional evidence of the uniqueness of the $Ag_4NEM_{14}$-MT complex; specifically, the Ag+ ions of the $Ag_i$-MT ($i = 9$–14) complexes are considerably more labile than are those of the $Ag_4$-MT in solution phase.

Chen and Russell previously showed that displacement of $Cd^{2+}$ from $Cd_7$-$MT^{5+}$ by NEM occurred by a two-component, cooperative mechanism' viz.' rapid displacement of three $Cd^{2+}$ ions followed by the slow loss of the remaining four $Cd^{2+}$ ions;[53] however, Shaw et al. reported $Cd^{2+}$ displacement by NEM is noncooperative based on the diminished NMR signal for both the $\alpha$- and $\beta$-domains.[72] Additional experimental results revealed that displacement of $Cd^{2+}$ by NEM was domain specific; the three $Cd^{2+}$ ions that are displaced first are from the $\beta$-domain, whereas subsequent $Cd^{2+}$ displacement is from the $\alpha$-domain.[53] $Ag_4$-MT is stable in NEM displacement, which further illustrates the uniqueness of its structure.

### Synthesis and Stabilities of Mixed Metal ($Ag^+/Cd^{2+}$) MT: Preferred Binding Domains for $Ag^+$ and $Cd^{2+}$.

The high abundance of $Ag_4$-MT product ions formed by titration of MT with $Ag^+$ ions is strikingly similar to that for titration of MT with $Cd^{2+}$ ions;[51] viz., $Ag_4$-MT appears to be formed cooperatively. This observation raises these questions: (i) does $Ag_4$-MT form a stable complex that is similar to $Cd_4$-MT or (ii) is this product domain specific? Our previous CID results of $Ag_4$-MT are interpreted as evidence that most of the fragmentations result in metal-containing y-type fragment ions and metal-free b-type fragment ions, which shows that four $Ag^+$ ions are more strongly interacting with cysteines in the $\alpha$-domain or are located in a region between two domains.[46] However, the CID results do not preclude the possibility that metal ions migrate to new binding sites prior to dissociation. In an effort to better understand the location of $Ag_4$-MT, cross metalation experiments were performed. These experiments were carried out by the addition of $Ag^+$ or $Cd^{2+}$ to aliquots of solutions containing MT (Figure 2A) to form $Ag_4$-MT (Figure 2B) and $Cd_4$-MT (Figure 2C), respectively. Following a short incubation period (1 h), $Cd^{2+}$ (Figure 2D) or $Ag^+$ (Figure 2E) was added to each solution. The final products of these reactions produced mixed metal complexes of $Ag_4Cd_4$-MT or $Cd_4Ag_4$-MT and low abundances of $Ag_5Cd_4$-MT or $Cd_4Ag_5$-MT, respectively. The $Ag_4Cd_4$-MT product was also formed by the addition of solutions containing equal concentrations of $Ag^+$ and $Cd^{2+}$ ions to a solution of MT (Figure 2F); thus, it appears that the formation of metalated products is independent of the order of metal addition. No metal replacement is observed.

### Top-Down and Bottom-Up Proteomics Following Covalent Labeling of $Ag_4$-MT with NEM: Where Are the $Ag^+$ Ions Bound?

Top-down proteomics sequencing strategies were combined with NEM labeling to further characterize $Ag_4$-MT. The addition of excess NEM to a solution containing $Ag_4$-MT (see Experimental Section) yielded $Ag_4NEM_{14}$-MT. The formation of this product suggests that, among the 20 cysteine residues in MT, 14 are labeled by NEM and the remaining 6 are coordinated to $Ag^+$ ions. CIU heat maps for $Ag_4NEM_{14}$-MT are shown in Figure 3A. The shifts in the CCS obtained by CIU are used to track the unfolding transition of the

$Ag_4NEM_{14}$-MT ions. The CCS of $Ag_4NEM_{14}$-MT is shifted from ~860 to ~880 $Å^2$ with collisional activation, but at higher collision energies (CEs), the CCS remains constant, indicating that the $Ag_4NEM_{14}$-MT complex resists unfolding. This result suggests that $Ag_4NEM_{14}$-MT is quite stable in the gas phase.

The $[Ag_4NEM_{14}\text{-MT}]^+$ ions were also analyzed by MS-CID-IM-MS (see the Experimental Section). Mass-selected $[Ag_4NEM_{14}\text{-MT}]^{5+}$ ions are activated by energetic collisions with a neutral gas atom (Ar), and the product ions formed are then analyzed by ion mobility (on the basis of size-to-charge) and mass spectrometry (on the basis of mass-to-charge) as illustrated in Figure 3B. The mass spectra shown in Figure 3C were obtained by extracting the ion signals bracketed by the dashed lines (marked with charge states) in Figure 3B. The fragment ions in each spectrum shown in Figure 3C are then used to assign the locations of the $Ag^+$ ions and NEM labels.

The most abundant CID fragment ions correspond to y-type fragment ions, viz., fragment ions formed by cleavage of the amide bond with charge retention by the C-terminus.[73] Assignments for the CID fragment ions of the $Ag_4NEM_{14}$-MT species are in Figure 3D. A series of metal-free, $\alpha$-domain CID fragments ranging from y2 to y29 also contain 1 to 11 NEM labeled residues and serve as evidence that none of the cysteine residues in the $\alpha$-domain are involved in $Ag^+$ binding (see Figure 3D). In addition, Cys5 and Cys7 are also labeled by NEM, which indicates that these sites are not involved in binding $Ag^+$ or that the metal binding is weak relative to other binding sites. Among the 7 cysteine residues between Cys13 and Cys29, 6 are involved in binding $Ag^+$ ions and one is labeled by NEM. The limited fragment ion coverage from Ser12 to Ser32 does not allow identification among Cys13 to Cys29; however, similar results for the $\beta$-domain discussed below help to resolve this issue.

IM-MS data of tryptic digested $Ag_4NEM_{14}$-MT were used to assign the $Ag^+$ binding sites of the $\beta$-domain. Tryptic digestion of $Ag_4NEM_{14}$-MT produced a number of peptides corresponding to cleavages of the $\alpha$-domain (see Figure S3 and Table S1) as well as tryptic fragments corresponding to the intact $\beta$-domain, viz., $m/z$ 1329.62 (3+) (GlySer-Met1-Lys30) containing four $Ag^+$ ions and three NEM labels. The CIU heat map (Figure S4A) suggests that the $Ag_4NEM_3$-$\beta$-domain$^{3+}$ is quite stable; viz., the complex does not unfold even at the highest CE, and the MS-CID-IM-MS data (Figure S4B,C) provide strong evidence that Cys5, Cys7, and Cys29 are bound to NEM and the four $Ag^+$ ions of the $Ag_4NEM_3$-domain are bound to Cys13, Cys15, Cys19, Cys21, Cys24. and Cys26.

Note that fragments from y3 to y9 contain one NEM and no $Ag^+$ ion, which suggests that, among Cys24, Cys26, and Cys29, only Cys29 is labeled by NEM. Cys24 and Cys26 are coordinated with $Ag^+$ ions, but the binding between these two cysteines and $Ag^+$ ions are relatively weak upon collisional activation. Lastly, missed tryptic cleavages at Lys20, Lys22, and Lys25 suggest that these residues are buried within a relatively stable $Ag_4Cys_6$ cluster, which is consistent with the CIU heat map (Figure S4A) for a high degree of stability of the $Ag_4Cys_6$ cluster.

The top-down/bottom-up proteomics analyses of the NEM labeled $Ag_4$-MT are interpreted as evidence that $Ag^+$ ions in this complex are located in the $\beta$-domain, specifically binding to Cys13, Cys15, Cys19, Cys21, Cys24, and Cys26. Palacios et al. previously reported that both $Ag^+$ and $Cu^+$ preferentially bind to the $\beta$-domain of MT to yield $M_6$-$\beta$MT.[19] Nielson and Winge,[74] Bofill et al.,[75] and Li and Otvos[76,77] also suggested that $Ag^+$ ions bind to the $\beta$-domain; however, Scheller et al. noted that "Experimentally, this was very hard to prove…".[20] The results of the NEM displacement reactions provide clear evidence that Ag+ ions of $Ag_4$-MT are bound in the $\beta$-domain, but the absence of a similar product, $Ag_6$-MT, appears to contradict these previous assignments. An alternative explanation could be that two of the Ag+ ions bound in the $\beta$-domain of $Ag_6$-MT are more weakly bound. We suggest that the weakly bound $Ag^+$ ions are possibly coordinated to Cys5, Cys7, and Cys29 and possibly bridging to Cys of the $\alpha$-domain.

The assignment by Palacios et al. of a stable Ag-MT complex was based on results obtained from UV–vis absorption, CD spectroscopy, and MS during the stepwise replacement of $Zn^{2+}$ by the addition of $Ag^+$ ions to solutions containing $Zn_7$-MT.[19] Using MS, they observed $Ag_4Zn_5$-MT and $Ag_4Zn_1$-$\beta$MT as the major product ions formed by the replacement of Zn by $Zn_7$-MT and $Zn_3$-$\beta$MT, respectively.[19] It is interesting to note that stable complexes with four $Cu^+$ ions have also been reported.[20,78] The integration of ESI-IM-MS, top-down and bottom-up proteomics with NEM labeling provides more definitive evidence regarding the $Ag^+$ ion binding sites and will be extended to the $Cu^+$ study.

## Collision-Induced Unfolding (CIU) of $Ag_j/Cd_i$MT and $Ag_i$-MT: Relative Stabilities of Metalated MT.

Results of the NEM displacement studies raise questions about the relative $Ag^+$-MT binding energies, but it is difficult to obtain accurate metal ion binding energies. Previous studies have shown that the sequential addition of metal ions to MTs promote formation of more compact structures,[46] and collision-induced dissociation (CIU) can be used to gain insights into how metalation changes the stabilities of the MT complex. Figure 4 contains CIU heat maps for the mixed metal complexes, i.e., $Ag_4Cd_4$-MT, $Ag_5Cd_4$-MT, $Cd_4Ag_4$-MT, and $Cd_4Ag_5$-MT. Prior to collisional activation, the CCS profile for $Ag_4Cd_4$-MT ions is centered at ~750 $Å^2$; CCS profiles at different CEs are contained in Figure S5. A portion of the ions unfold at ~75 eV ($E_{lab}$) to around 900 $Å^2$, while the CCS for the remaining ions is unchanged. Similar results are observed for $Cd_4Ag_4$-MT, except that $Cd_4Ag_4$-MT unfolds at lower activation energy than $Ag_4Cd_4$-MT. The CCS profile for $Ag_5Cd_4$-MT ions is centered at ~750 $Å^2$, but a population of $Ag_5Cd_4$-MT ions unfolds at ~100 eV to around 900 $Å^2$, while the majority stays folded upon collisional activation. Similar results are observed for $Cd_4Ag_5$-MT, except that $Cd_4Ag_5$-MT unfolds at a lower activation energy than does $Ag_5Cd_4$-MT. Intriguingly, the addition of $Cd^{2+}$ followed by the addition of $Ag^+$ and the addition of a $Ag^+/Cd^{2+}$ mixture to apo-MT yield almost identical CIU heat maps, whereas the addition of $Ag^+$ followed by the addition of $Cd^{2+}$ yields product ions that retain a higher abundance of the compact, folded conformers at all activation energies.

Note that the CIUs of $Cd_4Ag_4$- and $Ag_4Cd_4$-MT show some dependence on the order of metal addition. This effect is attributed to the influence of Cys33, which was previously

shown to be highly solvent exposed, and a weak binding site of $Cd^{2+}$ ions that can be displaced upon addition of NEM.[53,79] Cys33 may also have weak interactions with Ag+ in the formation of $Ag_4$-MT. With the addition of $Cd^{2+}$, the interaction between Cys33 and $Ag^+$ can be partially maintained. However, if $Cd^{2+}$ is added before $Ag^+$, the $Cd_4Cys_{11}$ cluster formed in the $a$-domain may inhibit interactions between $Ag^+$ and Cys33. As a result, MT metalated by $Ag^+$ and then by $Cd^{2+}$ produces a higher abundance of compact conformer than MT metalated by $Cd^{2+}$ first or by the $Ag^+/Cd^{2+}$ mixture.

CIU was also used to compare the gas-phase stabilities of the various $Ag_i$MT ($i = 4$–17) complexes (Figure 5).[46,62] CCS profiles for the $Ag_4$-MT ions are relatively broad and span the range from ~650 to 800 $\text{Å}^2$, and low abundance signals are observed as high as 950 $\text{Å}^2$ (see Figure S6). Similar to that observed for apo-MT, the width of the CCS profile is a signature for a conformationally disordered ion population.[46] As the CE is increased, the CCS of the ions increase to a maximum value of ~1000 $\text{Å}^2$. For example, at a CE of ~45 eV, the abundances of ions with a CCS of 750 $\text{Å}^2$ decreased and those in the range from ~850 $\text{Å}^2$ steadily increased; at a CE of approximately 60 eV, the abundances of ions with CCS ~ 950 $\text{Å}^2$ increased, and at a CE of ~75 eV, conformers reached a maximum CCS of ~1000 $\text{Å}^2$.

Although the CCSs for $Ag_5$-MT to $Ag_7$-MT show some differences, an intermediate state is observed across a narrow range of CE for $Ag_5$-MT. A similar state is observed for $Ag_6$- and $Ag_7$-MT, but this state appears to be more stable than that observed for $Ag_5$-MT. In fact, a state with a similar CCS (~875 $\text{Å}^2$) appears to be the final state for $Ag_8$-, $Ag_9$-, $Ag_{10}$-, and $Ag_{11}$-MT.

The CIU heat maps for $Ag_4$-MT through $Ag_7$-MT show considerable differences, whereas those for $Ag_8$-MT through $Ag_{11}$-MT are quite similar. At a low CE, the CCSs of $Ag_8$- to $Ag_{11}$-MT center on ~700 $\text{Å}^2$ and a maximum value ~850 $\text{Å}^2$ at the higher CEs; however, the threshold CE required to produce ions having the higher CCS increases as the number of bound $Ag^+$ ions increases from a CE value of ~55 eV for $Ag_4$-MT to ~110 eV for $Ag_{11}$-MT. For $Ag_{12}$-MT through $Ag_{17}$-MT, the CCS remains constant; for all of these ions, no change in CCS occurs as CE is increased. However, at high energies (200 eV), some of these ions begin to dissociate, without loss of $Ag^+$ ions.

There is a sharp drop in the CCSs for $Ag_{12}$-MT through $Ag_{17}$-MT. Zelazowski et al.,[21] Nielson and Winge,[74] and Li and Otvos[76] have shown that apo-MT requires at least 12 $Ag^+$ ions to fully metalate both domains, which is also supported by the results reported here. $Ag_{12}$-MT is resistant to unfolding because both domains are fully metalated. $Ag^+$ can adopt two different binding geometries with thiolates: trigonal and digonal.[1,17] For trigonal binding geometries, each $Ag^+$ ion interacts with three cysteines, whereas in digonal binding geometries, each $Ag^+$ ion interacts with two cysteines. The details of silver coordination are still open to debate. The only Ag+ metalated MT structure reported in the Protein Data Bank database for *Saccharomyces cerevisiae* was obtained by NMR. It appears that this system adopts a mixed coordination number of 2 and 3 for the seven bound Ag+ ions. Gui et al. investigated metal coordination of $Ag_{12}$-MT and $Ag_{17}$-MT from rabbit liver using K-edge X-ray absorption spectroscopy (XAS) and concluded that the $Ag^+$ ions in both $Ag_{12}$-MT and

$Ag_{17}$-MT are digonally coordinated by thiolates; the difference is that there are more bridging sulfurs in $Ag_{17}$-MT than in $Ag_{12}$-MT.[24] More recent work also using XAS by Veronesi et al. showed that Ag+ occupies trigonal sites mainly (~70%) for the same isoform. [25] Both geometry changes of $Ag^+$ and the fraction change of bridging and terminal sulfur may lead to the formation of $Ag_{17}$-MT from $Ag_{12}$-MT. The CCS profiles for $Ag_i$-MT ($i = 4$–17) under different activation energies are summarized in Figure S7.

Another possible mechanism for the formation of $Ag_{12}$- to $Ag_{17}$-MT is the influence of Ag–Ag interaction.[80,81] That is, the formation of Ag nanoclusters has been previously reported for nucleic acids/silver complexes,[82-84] and similar products may be formed by partially and/or fully metalated MTs. Studies are underway to explore whether silver nanoclusters are indeed formed in our ESI-MS experiments.

For comparison, ESI-MS spectra and CIU heat maps for $Ag_i$-rMT (rabbit MT) are provided as Figures S8 and S9, respectively. The CCSs for $Ag_i$-rMT are somewhat larger than those for $Ag_i$-MT, but CIU heat maps for $Ag_i$-rMT and $Ag_i$-MT show similar changes. Blindauer and Leszczyszyn state that the folding of MTs is dominated by metal binding and the formation of metal–cysteine clusters;[1] therefore, the structure should be mainly influenced by metal ions and cysteine residuals involved in metal binding. In our experiment, CIU heat maps during $Ag^+$ titration are quite similar for both types of MTs, which indicates similar stabilities of $Ag_i$-rMT and $Ag_i$-MT ($i = 4$–17). This is consistent with Blindauer and Leszczyszyn's statement.

## CONCLUSIONS

The comprehensive ESI-IM-MS approach employed here provides new insights about the metalation of human metallothionein-2A, both in terms of the metal ion binding sites and the relative stabilities of the $Ag_i$-MT complexes. Results from these studies provide clear evidence that $Ag^+$ ions of the Ag4-MT complex are bound in the $\beta$-domain. Bottom-up and top-down proteomics experiments clearly show that the $Ag^+$ ions are bound to Cys13, Cys15, Cys19, Cys21, Cys24, and Cys26, a binding arrangement that is very different from that of $Cd^{2+}$; viz., the $Cd^{2+}$ ions that react to form $Cd_4$-MT are located in the $\alpha$-domain.[45] This is also supported by results from studies with mixed metal ions ($Ag^+/Cd^{2+}$). However, results from collision-induced dissociation show that the unfolding process of $Ag_4Cd_4$-MT, $Cd_4Ag_4$-MT, $Ag_5Cd_4$-MT, and $Cd_4Ag_5$-MT is similar but not identical. The difference in unfolding may originate from some (see Figure 6) intramolecular interactions between the two domains with dependency on the order of metal ion addition. Overall, the combination of MS and IM (CIU) provides a comprehensive understanding of the relationship between $\alpha$- and $\beta$-domains. The different metal ion binding for these divalent and monovalent metal ions may be important in heavy metal detoxification and homeostasis involving different metal species.

Higher order $Ag_i$-MT clusters ($i = 5$–17) are formed when excess $Ag^+$ is added to solutions containing MT. Upon addition of N-ethylmalemide (NEM) to this solution, metal displacement produces $Ag_4NEM_{14}$-MT as the major product (>90%). This result is consistent with our assignment of higher binding energies of the four $Ag^+$ ions located in the

$\beta$-domain. Previous studies have reported compelling evidence for the formation of a $Ag_6$-MT, and it was suggested that all six $Ag^+$ ions are bound in the $\beta$-domain.[19,74, 76,77] Although we do not detect $Ag_6NEM_i$-MT complexes, we do feel that this observation contradicts the prior assignment of a stable $Ag_6$ cluster for $Ag_6$-MT. Instead, we suggest that in forming $Ag_6$ clusters, two $Ag^+$ ions are more weakly bound compared to the $Ag^+$ ions that bind to Cys13, Cys15, Cys19, Cys21, Cys24, and Cys26.

$Ag^+$ ions of $Ag_i$-MT ($i = 5$ to 14) can be displaced by NEM to form $Ag_4NEM_{14}$-MT. Such metal displacement was reported previously.[53,72] In those cases, the dissociation equilibrium of the metal–thiolate bond provides thiolate sites that are weakly associated with metal ions; those thiolate sites are reactive with NEM.[53,72] The $Ag^+$ ions that can be replaced by NEM are more labile in the solution phase.

## Supplementary Material

Refer to Web version on PubMed Central for supplementary material.

## ACKNOWLEDGMENTS

## REFERENCES

(1). Blindauer CA; Leszczyszyn OI Nat. Prod. Rep 2010, 27 (5), 720–741. [PubMed: 20442962]

(2). Capdevila M; Bofill R; Palacios O; Atrian S Coord. Chem. Rev 2012, 256 (1–2), 46–62.

(3). Scheller JS; Irvine GW; Stillman MJ Dalton T 2018, 47 (11), 3613–3637.

(4). Vallee BL Neurochem. Int 1995, 27 (1), 23–33. [PubMed: 7655345]

(5). Coyle P; Philcox JC; Carey LC; Rofe AM Cell. Mol. Life Sci 2002, 59 (4), 627–647. [PubMed: 12022471]

(6). Davis SR; Cousins RJ J. Nutr 2000, 130 (5), 1085–1088. [PubMed: 10801901]

(7). Kang YJ Exp. Biol. Med 2006, 231 (9), 1459–1467.

(8). Lu WH; Zelazowski AJ; Stillman MJ Inorg. Chem 1993, 32 (6), 919–926.

(9). Yang Y; Maret W; Vallee BL Proc. Natl. Acad. Sci. U. S. A 2001, 98 (10), 5556–5559. [PubMed: 11331777]

(10). Giles NM; Watts AB; Giles GI; Fry FH; Littlechild JA; Jacob C Chem. Biol 2003, 10 (8), 677–693. [PubMed: 12954327]

(11). Bell SG; Vallee BL ChemBioChem 2009, 10 (1), 55–62. [PubMed: 19089881]

(12). Petering DH; Mahim A Int. J. Mol. Sci 2017, 18 (6), 1289.

(13). Arseniev A; Schultze P; Worgotter E; Braun W; Wagner G; Vasak M; Kagi JHR; Wuthrich K J Mol. Biol 1988, 201 (3), 637–657.

(14). Narula SS; Mehra RK; Winge DR; Armitage IM J. Am. Chem. Soc 1991, 113 (24), 9354–9358.

(15). Blindauer CA; Harrison MD; Parkinson JA; Robinson AK; Cavet JS; Robinson NJ; Sadler PJ Proc. Natl. Acad. Sci. U. S. A 2001, 98 (17), 9593–9598. [PubMed: 11493688]

(16). Peroza EA; Schmucki R; Guntert P; Freisinger E; Zerbe O J. Mol. Biol 2009, 387 (1), 207–218. [PubMed: 19361445]

(17). Peterson CW; Narula SS; Armitage IM FEBS Lett. 1996, 379 (1), 85–93. [PubMed: 8566237]

(18). Calderone V; Dolderer B; Hartmann HJ; Echner H; Luchinat C; Del Bianco C; Mangani S; Weser U Proc. Natl. Acad. Sci. U. S. A 2005, 102 (1), 51–56. [PubMed: 15613489]

(19). Palacios O; Polec-Pawlak K; Lobinski R; Capdevila M; Gonzalez-Duarte P JBIC, J. Biol. Inorg. Chem 2003, 8 (8), 831–842. [PubMed: 14505073]

(20). Scheller JS; Irvine GW; Wong DL; Hartwig A; Stillman MJ Metallomics 2017, 9 (5), 447–462. [PubMed: 28466911]

(21). Zelazowski AJ; Gasyna Z; Stillman MJ J. Biol. Chem 1989, 264 (29), 17091–17099. [PubMed: 2793845]

(22). Scheuhammer AM; Cherian MG Toxicol. Appl. Pharmacol 1986, 82 (3), 417–425. [PubMed: 3952727]

(23). Bertini I; Hartmann HJ; Klein T; Liu GH; Luchinat C; Weser U Eur. J. Biochem 2000, 267 (4), 1008–1018. [PubMed: 10672009]

(24). Gui Z; Green AR; Kasrai M; Bancroft GM; Stillman MJ Inorg. Chem 1996, 35 (22), 6520–6529. [PubMed: 11666800]

(25). Veronesi G; Gallon T; Deniaud A; Boff B; Gateau C; Lebrun C; Vidaud C; Rollin-Genetet F; Carriere M; Kieffer I; Mintz E; Delangle P; Michaud-Soret I Inorg. Chem 2015, 54 (24), 11688–11696. [PubMed: 26632864]

(26). Yu XL; Wojciechowski M; Fenselau C Anal. Chem 1993, 65 (10), 1355–1359. [PubMed: 8517548]

(27). Fabris D; Zaia J; Hathout Y; Fenselau C J. Am. Chem. Soc 1996, 118 (48), 12242–12243.

(28). Kagi JHR; Vallee BL J. Biol. Chem 1960, 235 (12), 3460–3465. [PubMed: 13750713]

(29). Messerle BA; Schaffer A; Vasak M; Kagi JHR; Wuthrich K J. Mol. Biol 1990, 214 (3), 765–779. [PubMed: 2388267]

(30). Messerle BA; Schaffer A; Vasak M; Kagi JHR; Wuthrich K J. Mol. Biol 1992, 225 (2), 433–443. [PubMed: 1593628]

(31). Gehrig PM; You CH; Dallinger R; Gruber C; Brouwer M; Kagi JHR; Hunziker PE Protein Sci. 2000, 9 (2), 395–402. [PubMed: 10716192]

(32). Chassaigne H; Lobinski RJ Chromatogr A 1998, 829 (1–2), 127–136.

(33). Chassaigne H; Lobinski R Analyst 1998, 123 (10), 2125–2130. [PubMed: 10209897]

(34). Mounicou S; Polec K; Chassaigne H; Potin-Gautier M; Lobinski RJ Anal. At. Spectrom 2000, 15 (6), 635–642.

(35). Domenech J; Orihuela R; Mir G; Molinas M; Atrian S; Capdevila M JBIC, J. Biol. Inorg. Chem 2007, 12 (6), 867–882. [PubMed: 17503092]

(36). Orihuela R; Domenech J; Bofill R; You C; Mackay EA; Kagi JHR; Capdevila M; Atrian S JBIC, J. Biol. Inorg. Chem 2008, 13 (5), 801–812. [PubMed: 18389296]

(37). Domenech J; Bofill R; Tinti A; Torreggiani A; Atrian S; Capdevila M Biochim. Biophys. Acta, Proteins Proteomics 2008, 1784 (4), 693–704.

(38). Palacios O; Espart A; Espin J; Ding C; Thiele DJ; Atrian S; Capdevila M Metallomics 2014, 6 (2), 279–291. [PubMed: 24317230]

(39). Ngu TT; Stillman MJ J. Am. Chem. Soc 2006, 128 (38), 12473–12483. [PubMed: 16984198]

(40). Ngu TT; Easton A; Stillman MJ J. Am. Chem. Soc 2008, 130 (50), 17016–17028. [PubMed: 19053406]

(41). Sutherland DEK; Willans MJ; Stillman MJ J. Am. Chem. Soc 2012, 134 (6), 3290–3299. [PubMed: 22242602]

(42). Mierek-Adamska A; Dabrowska GB; Blindauer CA Metallomics 2018, 10 (10), 1430–1443. [PubMed: 30176031]

(43). Imam HT; Blindauer CA JBIC, J. Biol. Inorg. Chem 2018, 23 (1), 137–154. [PubMed: 29218630]

(44). M'kandawire E; Mierek-Adamska A; Sturzenbaum SR; Choongo K; Yabe J; Mwase M; Saasa N; Blindauer CA Int. J. Mol. Sci 2017, 18 (7), 1548.

(45). Chen SH; Russell WK; Russell DH Anal. Chem 2013, 85 (6), 3229–3237. [PubMed: 23421923]

(46). Dong SY; Wagner ND; Russell DH Anal. Chem 2018, 90 (20), 11856–11862. [PubMed: 30221929]

(47). Patrick JW; Gamez RC; Russell DH Anal. Chem 2015, 87 (1), 578–583. [PubMed: 25522119]

(48). Hopper JTS; Oldham NJ J. Am. Soc. Mass Spectrom 2009, 20 (10), 1851–1858. [PubMed: 19643633]

(49). Laganowsky A; Reading E; Allison TM; Ulmschneider MB; Degiacomi MT; Baldwin AJ; Robinson CV Nature 2014, 510 (7503), 172–175. [PubMed: 24899312]

(50). Wagner ND; Kim D; Russell DH Anal. Chem 2016, 88 (11), 5934–5940. [PubMed: 27137645]

(51). Chen SH; Chen LX; Russell DH J. Am. Chem. Soc 2014, 136 (26), 9499–9508. [PubMed: 24918957]

(52). Chen SH; Russell DH J. Am. Soc. Mass Spectrom 2015, 26 (9), 1433–1443. [PubMed: 26115967]

(53). Chen SH; Russell DH Biochemistry 2015, 54 (39), 6021–6028. [PubMed: 26375382]

(54). Wagner ND; Russell DH J. Am. Chem. Soc 2016, 138 (51), 16588–16591. [PubMed: 27977175]

(55). Hogstrand C; Galvez F; Wood CM Environ. Toxicol. Chem 1996, 15 (7), 1102–1108.

(56). Osobova M; Urban V; Jedelsky PL; Borovicka J; Gryndler M; Ruml T; Kotrba P New Phytol. 2011, 190 (4), 916–926. [PubMed: 21261626]

(57). Han LJ; Hyung SJ; Mayers JJS; Ruotolo BT J. Am. Chem. Soc 2011, 133 (29), 11358–11367. [PubMed: 21675748]

(58). Tian YW; Han LJ; Buckner AC; Ruotolo BT Anal. Chem 2015, 87 (22), 11509–11515. [PubMed: 26471104]

(59). Watanabe Y; Vasiljevic S; Allen JD; Seabright GE; Duyvesteyn HME; Doores KJ; Crispin M; Struwe WB Anal. Chem 2018, 90 (12), 7325–7331. [PubMed: 29757629]

(60). Tian YW; Ruotolo BT Int. J. Mass Spectrom 2018, 425, 1–9.

(61). Tian YW; Ruotolo BT Analyst 2018, 143 (11), 2459–2468. [PubMed: 29736508]

(62). Dixit SM; Polasky DA; Ruotolo BT Curr. Opin. Chem. Biol 2018, 42, 93–100. [PubMed: 29207278]

(63). Zinnel NF; Pai PJ; Russell DH Anal. Chem 2012, 84 (7), 3390–3397. [PubMed: 22455956]

(64). Zinnel NF; Russell DH Anal. Chem 2014, 86 (10), 4791–4798. [PubMed: 24754452]

(65). McLean JA; Ruotolo BT; Gillig KJ; Russell DH Int. J. Mass Spectrom 2005, 240 (3), 301–315.

(66). Eschweiler JD; Rabuck-Gibbons JN; Tian YW; Ruotolo BT Anal. Chem 2015, 87 (22), 11516–11522. [PubMed: 26489593]

(67). Polasky DA; Dixit SM; Fantin SM; Ruotolo BT Anal. Chem 2019, 91 (4), 3147–3155. [PubMed: 30668913]

(68). Testa L; Brocca S; Grandori R Anal. Chem 2011, 83 (17), 6459–6463. [PubMed: 21800882]

(69). Grabenauer M; Wyttenbach T; Sanghera N; Slade SE; Pinheiro TJT; Scrivens JH; Bowers MT J. Am. Chem. Soc 2010, 132 (26), 8816–8818. [PubMed: 20536231]

(70). Pai PJ; Cologna SM; Russell WK; Vigh G; Russell DH Anal. Chem 2011, 83 (7), 2814–2818. [PubMed: 21395231]

(71). Salgado MT; Bacher KL; Stillman MJ JBIC, J. Biol. Inorg. Chem 2007, 12 (3), 294–312. [PubMed: 17086417]

(72). Shaw CF; He LB; Munoz A; Savas MM; Chi S; Fink CL; Gan T; Petering DH JBIC, J. Biol. Inorg. Chem 1997, 2 (1), 65–73.

(73). Roepstorff P; Fohlman J Biomed. Mass Spectrom 1984, 11 (11), 601–601. [PubMed: 6525415]

(74). Nielson KB; Winge DR J. Biol. Chem 1985, 260 (15), 8698–8701. [PubMed: 4019449]

(75). Bofill R; Palacios O; Capdevila M; Cols N; Gonzalez-Duarte R; Atrian S; Gonzalez-Duarte PJ Inorg. Biochem 1999, 73 (1–2), 57–64.

(76). Li H; Otvos JD Biochemistry 1996, 35 (44), 13929–13936. [PubMed: 8909290]

(77). Li H; Otvos JD J. Inorg. Biochem 1998, 70 (3–4), 187–194. [PubMed: 9720304]

(78). Jensen LT; Peltier JM; Winge DR JBIC, J. Biol. Inorg. Chem 1998, 3 (6), 627–631.

(79). Robbins AH; Mcree DE; Williamson M; Collett SA; Xuong NH; Furey WF; Wang BC; Stout CD J. Mol. Biol 1991, 221 (4), 1269–1293. [PubMed: 1942051]

(80). Hu SQ; Ye BY; Yi XY; Cao ZZ; Wu DH; Shen CC; Wang JX Talanta 2016, 155, 272–277. [PubMed: 27216684]

(81). Cui YY; Wang YL; Zhao LN Small 2015, 11 (38), 5118–5125. [PubMed: 26248576]

(82). Choi S; Yu JH APL Mater. 2017, 5 (5), 053401.

(83). Sych TS; Reveguk ZV; Pomogaev VA; Buglak AA; Reveguk AA; Ramazanov RR; Romanov NM; Chikhirzhina EV; Polyanichko AM; Kononov AI J. Phys. Chem. C 2018, 122 (51), 29549–29558.

(84). Huard DJE; Demissie A; Kim D; Lewis D; Dickson RM; Petty JT; Lieberman RL J. Am. Chem. Soc 2019, 141, 11465. [PubMed: 30562465]
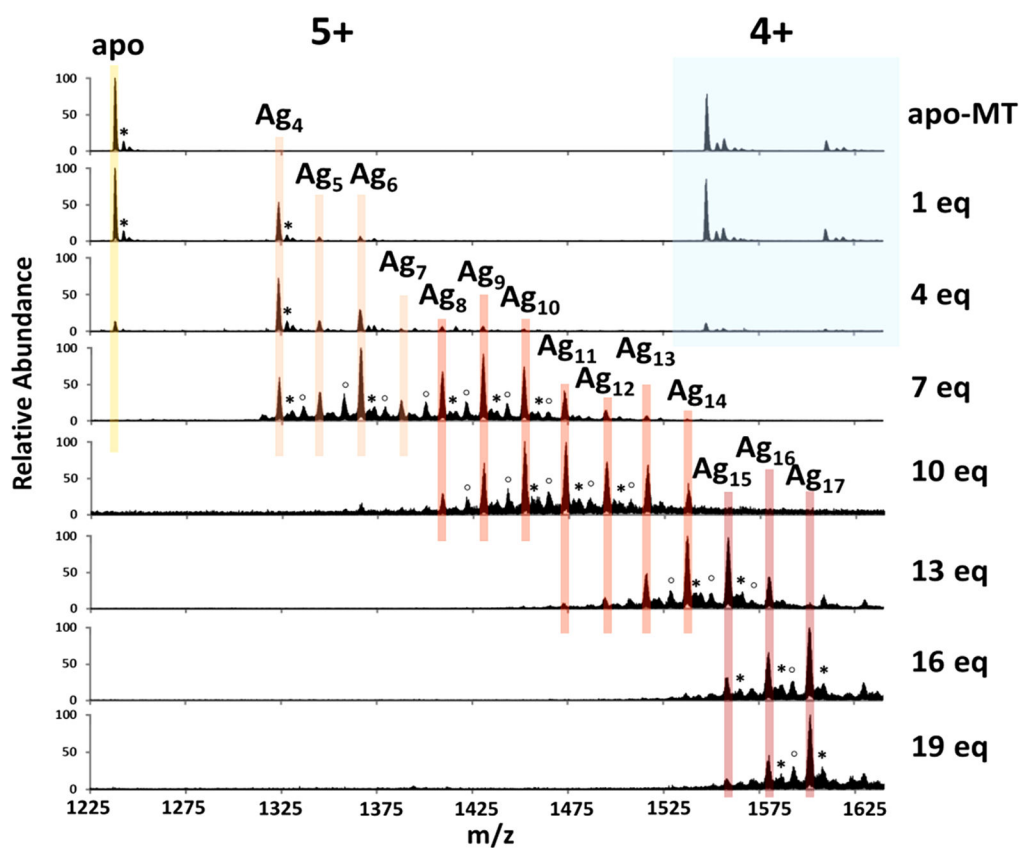
**Figure 1.**
ESI-MS spectra taken following sequential addition of Ag$^+$ to apo-MT solution. Peaks with asterisks (*) and circles (○) are for ions that shifted by ~23 and ~60 Da, corresponding to sodium and acetate adducts, respectively.
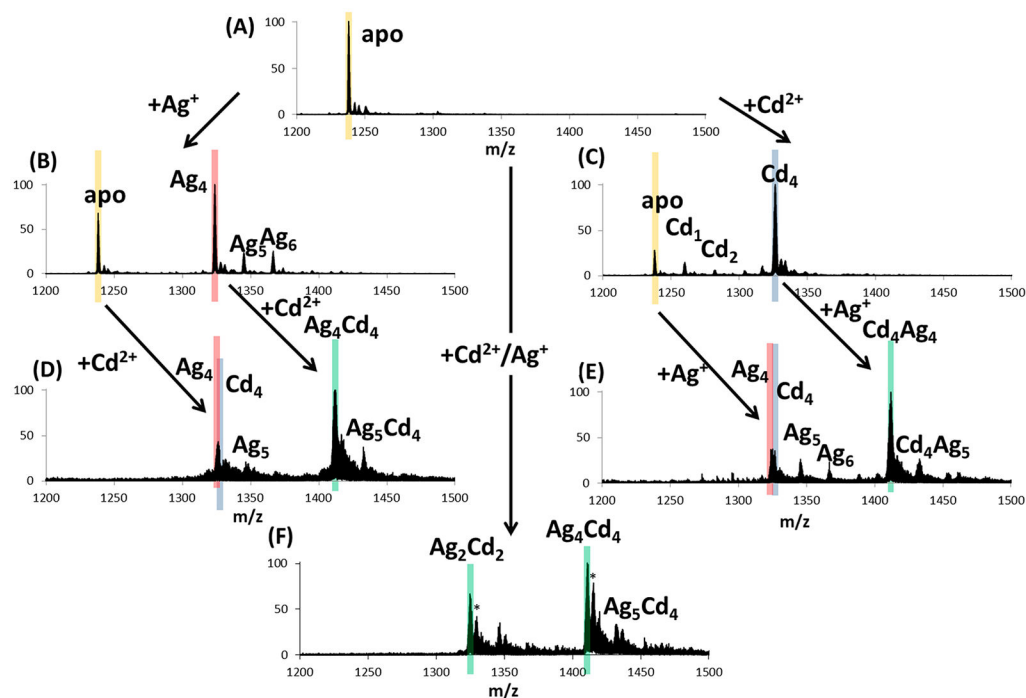
**Figure 2.**
Mass spectra of MT obtained following the addition of $Cd^{2+}/Ag^+$ ions. (A) apo-MT; (B) after addition of four equiv $Ag^+$; (C) after addition of four equiv $Cd^{2+}$; (D) addition of four equiv $Cd^{2+}$ to a solution of $Ag_i$-MT; (E) addition of four equiv $Ag^+$ to a solution of $Cd_i$-MT; (F) apo-MT reacted with a $Ag^+/Cd^{2+}$ mixture. Peaks with an asterisk (*) are for $Na^+$ adducts. The peaks in (D) and (E) labeled in red can be assigned as $Ag_4$-MT. The peaks labeled in blue can be assigned as $Cd_4$-MT. $Ag_2Cd_2$-MT in (F) is assigned as one MT binding two $Ag^+$ and two $Cd^{2+}$. The identification is limited by the resolution of the instrument. A zoomed-in isotopic distribution is shown in Figure S2.
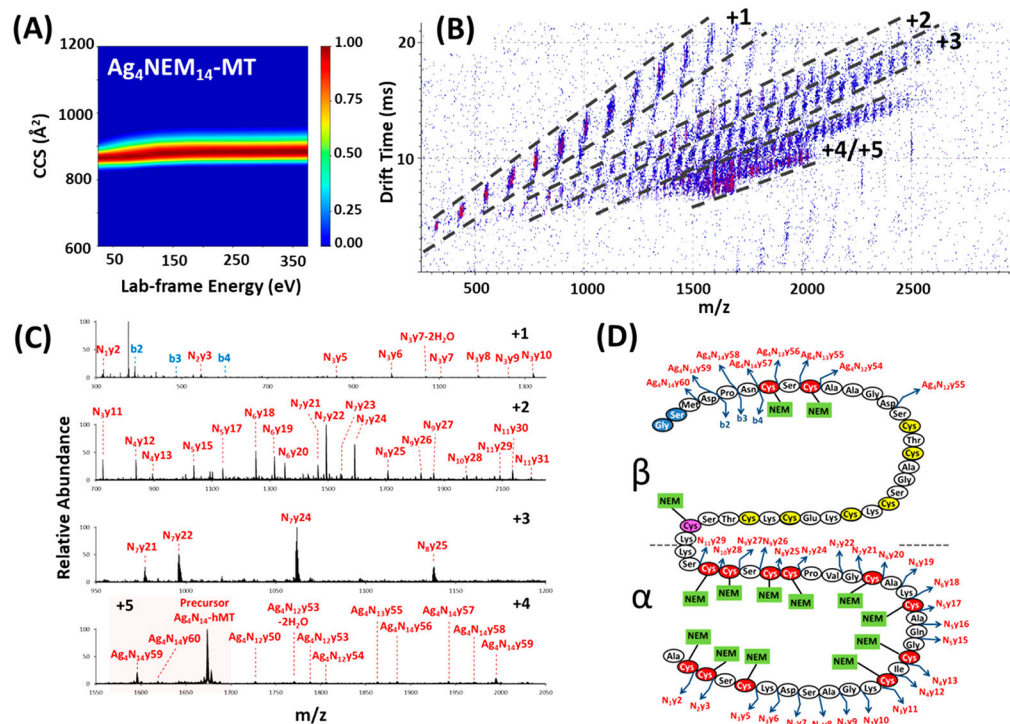
**Figure 3.**
(A) CIU of $Ag_4NEM_{14}$-MT. Due to the limited fragmentation coverage from Ser12 to Ser32, 13 (colored in red) out of the 14 NEM labeled cysteines can be located with the top-down approach. Cys29 (colored in pink) is proved to be NEM labeled later with the bottom-up approach. (B) 2D MS-CID-IM-MS spectrum of $A_4NEM_{14}$-MT. The trend lines are shown for ions of different charge states as labeled (+1 to +5). (C) Extracted mass spectra for each trend line; for simplicity, NEM is abbreviated as "N". (D) Summary of the identified fragment ions and corresponding model from panel C. The labels $\alpha$ and $\beta$ indicate the location of the domains. The N-terminal GlySer-tag, a product of tag cleavage using the TEV protease, is not included in the amino acid position assignments.
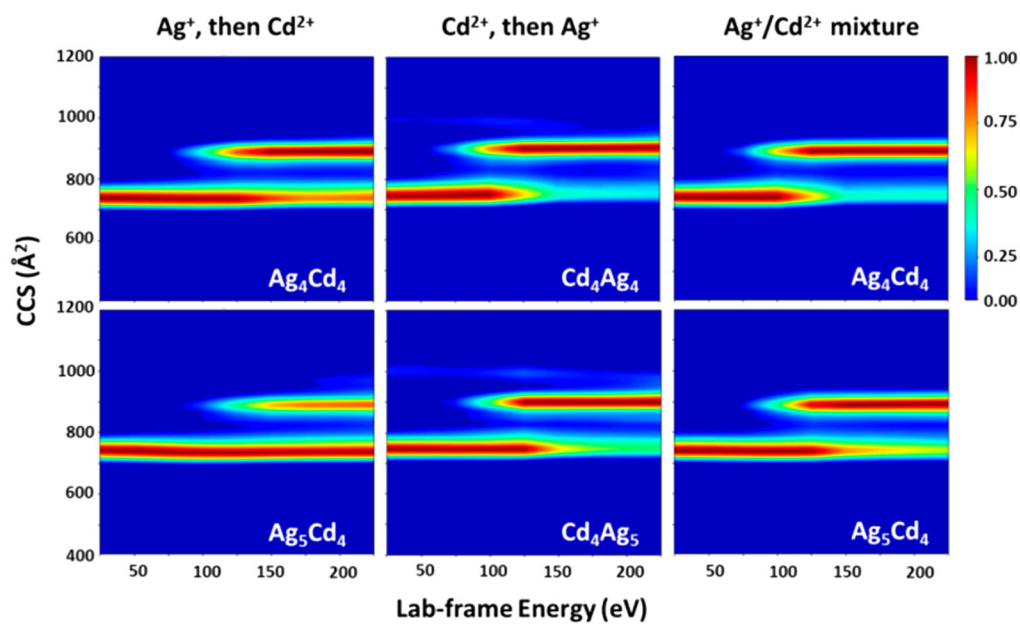
**Figure 4.**
Collision-induced unfolding (CIU) heat maps for $Ag_4Cd_4$-MT, $Ag_4Cd_4$-MT, $Cd_4Ag_4$-MT, and $Cd_4Ag_5$-MT. The legends at the top of each panel provide the sequence of the addition of each metal ion.
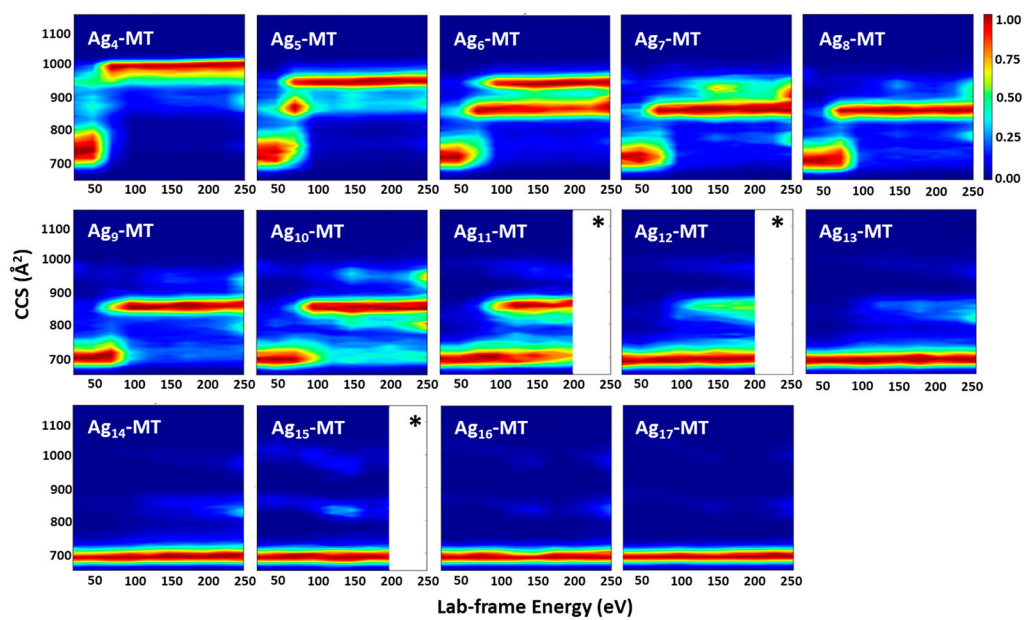
**Figure 5.**
CIU heat maps for Ag4-MT to Ag17-MT. Asterisks (*) indicate that the CIU heat maps are truncated due to collision-induced dissociation. CID forms fragmentations from the N-terminus; no $Ag^+$ dissociation is detected.
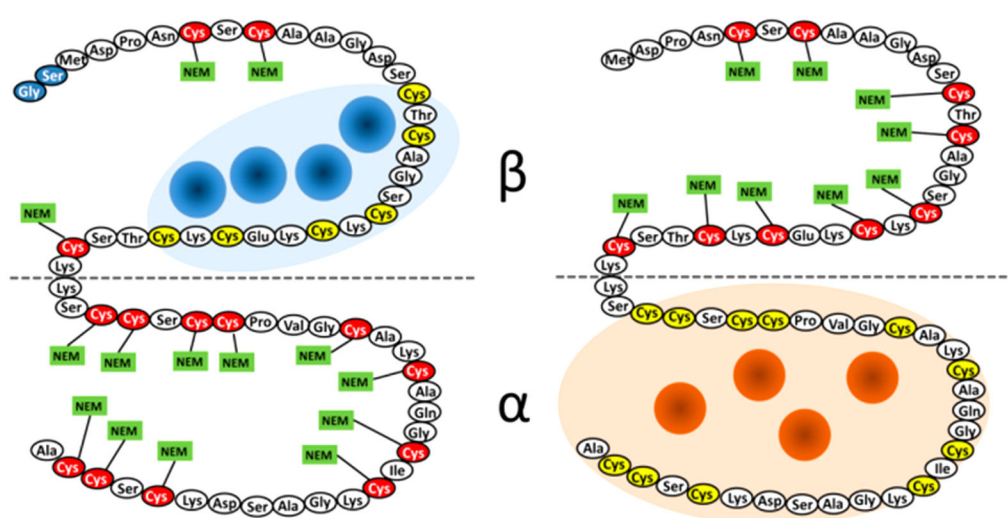
**Figure 6.**
Summary of binding sites identification. $Ag^+$ ions (blue) of $Ag_4$-MT are located in the $\beta$-domain, whereas $Cd^{2+}$ ions (orange) of $Cd_4$-MT are located in the $\alpha$-domain. The binding sites for $Cd_4$-MT are summarized from a previous publication.[45]